AIAA JOURNAL
Vol. 40, No. 11, November 2002

Development of Curvature Sensitive Nonlinear Eddy-Viscosity Model

S. Fu* and W. Q. Qian†
Tsinghua University, Beijing 100084, People's Republic of China

Current widely used turbulence closures, except the full second-moment closure, cannot properly account for the suppression of turbulence by convex curvature and the enhancing effect by concave curvature. Particularly, the failure of the explicit algebraic stress model (EASM) to capture the curvature strain effects in curved flows can be attributed to the equilibrium assumption embodied in EASM. Thus, the algebraic stress model (ASM) approach is reexamined in the framework of a generalized curvilinear coordinate system. In the approach, the equilibrium assumption applies only to the gradient part of convective transport while the curvature-related algebraic terms in the Reynolds stress convection process are retained. In this way, a curvature sensitive ASM is derived and is further transformed into an explicit nonlinear eddy-viscosity model in an orthogonal coordinate system. With this newly developed explicit ASM to predict the curved flow in a two-dimensional U duct, it is observed that the turbulence suppression at the convex wall is successfully captured.

Nomenclature

b^{ij} = Reynolds stress anisotropy tensor
C^{ij} = physical component of $\hat{C}^{ij}$
$\hat{C}^{ij}$ = contravariant form of Reynolds stress convection
$C^{ij}_{(G)}$ = gradient part of C^{ij}
$C^{ij}_{(R)}$ = curvature sensitive part of C^{ij}
D^{ij} = physical component of $\hat{D}^{ij}$
$\hat{D}^{ij}$ = contravariant form of Reynolds stress diffusion
g = determinant of g_{ij}
g^{ij} = contravariant metric tensor
g_{ij} = covariant metric tensor, $(\partial x^m/\partial y^i)(\partial x^m/\partial y^j)$
H = duct height
k = turbulent kinetic energy
P^{ij} = physical component of $\hat{P}^{ij}$
$\hat{P}^{ij}$ = contravariant form of Reynolds stress generation
r = radial coordinate in the circular section of U duct
S^{ij} = mean strain rate
s = coordinate along U-duct centerline; 0 at duct entrance
U^i = physical component of the mean contravariant velocity V^i
$\tilde{U}^i$ = instantaneous physical component of $\hat{v}^i$
U_0 = average inlet flow velocity
u^i = physical component of fluctuating contravariant velocity v^i
$\overline{u^i u^j}$ = physical component of contravariant Reynolds stress
V^i = mean contravariant velocity component
v^i = fluctuating contravariant velocity component
$\hat{v}^i$ = instantaneous contravariant velocity component $\tilde{U}^i/\sqrt{g_{ii}}$ (no summary on i)
$\overline{v^i v^j}$ = contravariant Reynolds stress
W^{ij} = mean flow vorticity
W'^{ij} = new effective vorticity
Γ_{ijk} = Christoffel symbol of the first kind, $[ij,k] \equiv \frac{1}{2}[(\partial g_{ik}/\partial x^j) + (\partial g_{jk}/\partial x^i) - (\partial g_{ij}/\partial x^k)]$
Γ^k_{ij} = Christoffel symbol of the second kind

$$\left\{ \begin{matrix} k \\ i \quad j \end{matrix} \right\} \equiv g^{k\alpha}[ij,\alpha] = g^{k\alpha}\Gamma_{ij\alpha}$$

δ^{ij} = Kronecker delta
ϵ = dissipation rate of turbulent kinetic energy
ϵ^{ij} = physical component of $\hat{\epsilon}^{ij}$
$\hat{\epsilon}^{ij}$ = contravariant form of Reynolds stress dissipation
θ = tangential coordinate in the circular section of U-duct
τ^{12} = Reynolds shear stress
Φ^{ij} = physical component of $\hat{\Phi}^{ij}$
$\hat{\Phi}^{ij}$ = contravariant form of Reynolds stress redistribution
ω^{ij} = additional term of vorticity deduced from $C^{ij}_{(R)}$

I. Introduction

FLOWS in engineering applications often occur in curved geometry, for example, curved channels, ducts and pipes, bends, and curved surfaces. In computational fluid dynamics study of these flows, it is usually desirable to adopt a form of body-fitted and orthogonal grids to ensure that the boundary condition be applied properly and to achieve higher numerical accuracy. In terms of the flow physics, curved turbulent flows are known to exhibit features distinct from flows with simple shear.[1–3] Flows over convex surfaces experience suppression on the turbulence level that can be so strong as to cause flow relaminarization.[4] Concave surfaces, on the other hand, enhance flow turbulence. Thus, appropriately resolving these delicate curvature effects on turbulent flows can be of crucial relevance to the success of numerical calculation of flows with curved geometry.

It is well known, however, that the current widely used low-level turbulence closures, for example, the series of one-equation and two-equation eddy-viscosity models, are insensitive to curvature and that only the cubic nonlinear eddy-viscosity can capture the effect of streamline curvature to some extent.[5] For the explicit algebraic stress model (EASM), which was developed by Pope[6] and Gatski and Speziale[7] and believed to possess more physics in the model structure, it is observed by Rumsey et al.[8] and Luo and Lakshminarayana[9] that this quadratic nonlinear eddy-viscosity model also fails to capture the curvature strain effect. This failure was attributed by Rumsey et al.[8] to the equilibrium assumption $Db^{ij}/Dt = 0$, embodied in the EASM. They put forward the idea of assuming anisotropy equilibrium in the reference frame defined by the principle axes of the strain rate tensor,[10] that is, replacing the assumption of $Db^{ij}/Dt = 0$ with $D\bar{b}^{ij}/Dt = 0$, where $\bar{b}^{ij}$ is the transformed anisotropy tensor in the principle axes coordinate frame. Numerical results show that this

Received 10 January 2002; revision received 27 May 2002; accepted for publication 4 June 2002.

*Professor, Department of Engineering Mechanics; fs-dem@mail.tsinghua.edu.cn.
†Postdoctor, Department of Engineering Mechanics.

modification is valid in the curved region of the flowfield, but only somewhat minor improvement is achieved in the calculated profile of shear stress and skin-friction profiles.[10]

It also has been suggested by Rodi and Scheurer[11] that the weak equilibrium assumption is better evaluated for the anisotropy tensor expressed in a streamline-based coordinate system. In cases with modestly curved streamlines, the choice of coordinate system has a rather minor effect; however, in cases with strong streamline curvature, this effect is dominating. Thus, Girimaji[12] suggested application of the weak-equilibrium assumption in a flow acceleration coordinate system, and this led to a Galilean invariant EASM for curved flows. Wallin and Johansson[13] recently further developed this idea and obtained a simplified form of this Galilean-invariant EASM. However, in Girimaji's and Wallin and Johansson's EASM, the values of acceleration vector and the rate of change of acceleration vector are to be calculated. This point is likely to hinder their further application in engineering flow calculations.

On the other hand, in the study of swirling curved flows, a number of investigations have illustrated that the algebraic stress model (ASM) assumption causes the loss of swirl-related curvature terms that appear naturally in the cylindric coordinates.[14,15] Even in the second-moment closure, these curvature terms were found to play an important role in the pressure–strain model. For instance, Gibson and Younis[15] were able to obtain improved computational results when the curvature terms were "pressure-scrambled" to enhance the swirl effect.

In the present work, the ASM approach is reexamined in the framework of a generalized curvilinear coordinates system that is usually adopted to describe arbitrary flow geometry. The curvature-related algebraic terms in the Reynolds stress convection process are retained, and the equilibrium assumption applies only to the genuine convective transport, the gradient part. In this way, a curvature sensitive ASM is derived and is further transformed into an explicit orthogonal form denoted as curvature-modified EASM (EASM-C) in the following analysis. The use of the orthogonality condition stems from two considerations: 1) significant reduction in the complexity of the curvature sensitive EASM formulation and 2) better numerical accuracy. The newly developed EASM-C is applied to the prediction of the flow in the two-dimensional U duct. It is observed that the turbulence suppression at the convex wall is successfully captured with EASM-C.

II. Flow Governing Equations in Contravariant Forms

In the present study, the flow is assumed to be incompressible and isothermal with constant viscosity. The instantaneous flow governing equations are written in contravariant tensor form to keep them form invariant in an arbitrary coordinate system. Based on these contravariant equation forms, transformation of the coordinate system fitted to any curved flow geometries can appropriately provide deeper understanding of the effect of curvature on the turbulent flow.

The derivation of the following equations requires extensive tensor analysis. For a detailed description of this subject and its application in fluid mechanics, readers are referred to the textbooks on tensor and continuum mechanics, for example, that by Sokolnikoff.[16]

A. Continuity Equation

The continuity equation in contravariant form can be written as

$$\hat{v}^i_{,i} = 0 \tag{1}$$

In expanded contravariant form, Eq. (1) can be further written as

$$\frac{\partial \hat{v}^i}{\partial x^i} + \Gamma^i_{ki}\hat{v}^k = 0 \tag{2}$$

From the theory of tensor it can be shown $\Gamma^i_{ki} = \partial(\ell n\sqrt{g})/\partial x^k$; hence, the continuity equation can also be written as

$$\frac{\partial \hat{v}^i}{\partial x^i} + \hat{v}^k\frac{\partial\left(\ell n\sqrt{g}\right)}{\partial x^k} = 0 \tag{3}$$

where g is the determinant of g_{ij}, that is, $g = |g_{ij}|$.

B. Navier–Stokes Equations

The Navier–Stokes equation in contravariant form can be written as

$$\hat{v}^i_{,t} + \hat{v}^k\hat{v}^i_{,k} = -(1/\rho)g^{ki}\hat{p}_{,k} + \nu\hat{v}^i_{,kl}g^{kl} \tag{4}$$

In expanded form it reads

$$\frac{\partial \hat{v}^i}{\partial t} + \hat{v}^k\left(\frac{\partial \hat{v}^i}{\partial x^k} + \Gamma^i_{kl}\hat{v}^l\right) = -\frac{1}{\rho}g^{ki}\hat{p}_{,k} + \nu g^{kl}\left[\frac{\partial^2\hat{v}^i}{\partial x^k\partial x^l} + \Gamma^i_{kp}\frac{\partial \hat{v}^p}{\partial x^l} + \Gamma^i_{lp}\frac{\partial \hat{v}^p}{\partial x^k} - \Gamma^p_{lk}\frac{\partial \hat{v}^i}{\partial x^p} + \left(\frac{\partial\Gamma^i_{lp}}{\partial x^k} + \Gamma^i_{mk}\Gamma^m_{pl} - \Gamma^i_{pm}\Gamma^m_{lk}\right)\hat{v}^p\right] \tag{5}$$

In Eq. (5), all of the terms related to the Christoffel symbol are curvature terms. It is understood here that the term related to the Christoffel symbol on the left-hand side of the equation denotes the curvature acceleration and that the Christoffel symbol terms on the right-hand side represent curvature modifications to the viscous diffusion in the Navier–Stokes equation.

C. Ensemble-Averaged Flow Equations

In turbulent flows, the continuity and momentum equations just presented describe the instantaneous flowfield. Following the well-known Reynolds decomposition procedure, the instantaneous flow quantity, for instance, the contravariant velocity component $\hat{v}^i$, becomes

$$\hat{v}^i = V^i + v^i \tag{6}$$

Hence, the mean and the fluctuating continuity equations are

$$V^i_{,i} = 0, \qquad v^i_{,i} = 0 \tag{7}$$

The ensemble-averaged Navier–Stokes equation in the contravariant form, therefore, can be written as

$$V^i_{,t} + V^kV^i_{,k} = -(1/\rho)g^{ki}P_{,k} + \nu g^{kl}V^i_{,kl} - (\overline{v^iv^k})_{,k} \tag{8}$$

The last term in Eq. (8), commonly known as Reynolds stress in contravariant form, occurs as a result of ensemble averaging.

D. Reynolds Stress Transport Equations

1. Contravariant Forms

The Reynolds stress transport equations can be readily derived from the Navier–Stokes equations. The detailed derivation procedures are omitted here, only the final equation in the contravariant form is given:

$$\hat{C}^{ij} = (\overline{v^iv^j})_{,t} + V^k(\overline{v^iv^j})_{,k} = \hat{D}^{ij} + \hat{P}^{ij} + \hat{\Phi}^{ij} - \hat{\epsilon}^{ij} \tag{9}$$

where

$$\hat{D}^{ij} = \left[\nu g^{kl}(\overline{v^iv^j})_{,l} - g^{ik}\overline{pv^j}/\rho - g^{jk}\overline{pv^i}/\rho - \overline{v^iv^jv^k}\right]_{,k}$$

$$\hat{P}^{ij} = -\overline{v^iv^k}V^j_{,k} - \overline{v^jv^k}V^i_{,k}$$

$$\hat{\Phi}^{ij} = \left[g^{ik}(\overline{pv^j})_{,k} + g^{jk}(\overline{pv^i})_{,k}\right]\Big/\rho$$

$$\hat{\epsilon}^{ij} = 2\nu g^{kl}\overline{v^i_{,k}v^j_{,l}} \tag{10}$$

The terms $\hat{C}^{ij}$, $\hat{D}^{ij}$, $\hat{P}^{ij}$, $\hat{\Phi}^{ij}$, and $\hat{\epsilon}^{ij}$, in Eq. (10) represent stress convection, diffusion, generation, redistribution, and dissipation, respectively.

Equation (9) provides the Reynolds stress transport equation in the contravariant form. To appreciate the curvature effects on the Reynolds stresses, it is necessary to examine the equation in the expanded form. Here, attention will be focused on the stress convection and generation terms because the diffusion term often plays a minor part in the stress transport process. The expansion of the convection term can be written as

$$\hat{C}^{ij} = \frac{\partial\overline{v^iv^j}}{\partial t} + V^k\left(\frac{\partial\overline{v^iv^j}}{\partial x^k} + \Gamma^i_{lk}\overline{v^lv^j} + \Gamma^j_{lk}\overline{v^lv^i}\right) \tag{11}$$

The stress generation rate written in the expanded contravariant form reads

$$\hat{P}^{ij} = -\overline{v^i v^k}\left(\frac{\partial V^j}{\partial x^k} + \Gamma^j_{lk} V^l\right) - \overline{v^j v^k}\left(\frac{\partial V^i}{\partial x^k} + \Gamma^i_{lk} V^l\right) \tag{12}$$

Note that the curvature terms related to the Christoffel symbol Γ^i_{jk} are identical in both $\hat{C}^{ij}$ and $\hat{P}^{ij}$ expressions but with opposite signs.

2. Physical Componental Forms

For application, the preceding analysis based on the contravariant forms needs be transformed into the corresponding physical componental forms. The relationship between the contravariant Reynolds stresses $\overline{v^i v^j}$ and their counterparts in physical components $\overline{u^i u^j}$ is

$$\overline{v^i v^j} = \frac{\overline{u^i u^j}}{\sqrt{g_{ii} g_{jj}}} \qquad \text{or} \qquad \overline{u^i u^j} = \sqrt{g_{ii} g_{jj}}\,\overline{v^i v^j} \tag{13}$$

Thus, the physical component form of the Reynolds stress equations can be written as

$$C^{ij} = D^{ij} + P^{ij} + \Phi^{ij} - \varepsilon^{ij} \tag{14}$$

where

$$C^{ij} = \sqrt{g_{ii} g_{jj}}\hat{C}^{ij}, \qquad D^{ij} = \sqrt{g_{ii} g_{jj}}\hat{D}^{ij}, \qquad P^{ij} = \sqrt{g_{ii} g_{jj}}\hat{P}^{ij}$$

$$\Phi^{ij} = \sqrt{g_{ii} g_{jj}}\hat{\Phi}^{ij}, \qquad \epsilon^{ij} = \sqrt{g_{ii} g_{jj}}\hat{\epsilon}^{ij}$$

Because we are only interested in the convection term, the expanded form has the following expression:

$$C^{ij} = \underbrace{\frac{\partial \overline{u^i u^j}}{\partial t} + \frac{U^k}{\sqrt{g_{kk}}}\frac{\partial \overline{u^i u^j}}{\partial x^k}}_{C^{ij}_{(G)}} \underbrace{-\overline{u^i u^j}\frac{\partial\left(\ell_n \sqrt{g_{ii} g_{jj}}\right)}{\partial t}}_{C^{ij}_{(T)}}$$

$$\underbrace{-\overline{u^i u^j}\frac{U^k}{\sqrt{g_{kk}}}\frac{\partial\left(\ell_n \sqrt{g_{ii} g_{jj}}\right)}{\partial x^k} + \frac{U^k}{\sqrt{g_{kk}}}\left(\Gamma^i_{kl}\sqrt{\frac{g_{ii}}{g_{ll}}}\overline{u^l u^j} + \Gamma^j_{kl}\sqrt{\frac{g_{jj}}{g_{ll}}}\overline{u^i u^l}\right)}_{C^{ij}_{(R)}} \tag{15}$$

For many practical applications, the coordinate systems are independent of time, that is, $C^{ij}_{(T)} = 0$. The preceding expression, thus, shows that in the generalized curvilinear coordinate system the convection of Reynolds stresses consists of two components: the gradient term $C^{ij}_{(G)}$ and the curvature term $C^{ij}_{(R)}$, that is, $C^{ij} = C^{ij}_{(G)} + C^{ij}_{(R)}$.

III. Derivation of Curvature Sensitive Nonlinear Eddy-Viscosity Model

A. Curvature Terms

The curvature term $C^{ij}_{(R)}$ shown in expression (15) is algebraic in the Reynolds stresses. The contraction of the indices i and j of this curvature term gives

$$C^{ll}_{(R)} = -\frac{U^k}{\sqrt{g_{kk}}}\left[\overline{u^l u^l}\frac{\partial(\ell_n g_{ll})}{\partial x^k} - 2\Gamma^l_{ks}\sqrt{\frac{g_{ll}}{g_{ss}}}\overline{u^s u^l}\right] \tag{16}$$

From the mathematical formality (Appendix A), an important property of this contraction in the orthogonal curvilinear coordinate system is

$$C^{ll}_{(R)} = 0 \tag{17}$$

For instance, in the cylindric polar coordinate system, it is known that the curvature term $C^{ij}_{(R)}$ in the componental form can be written as

$$C^{zz}_{(R)} = 0, \qquad C^{rr}_{(R)} = -C^{\theta\theta}_{(R)} = 2\overline{u^r u^\theta}(U^\theta/r)$$

$$C^{zr}_{(R)} = (\overline{u^r u^r} - \overline{u^\theta u^\theta})U^\theta/r \tag{18}$$

that is, $C^{zz}_{(R)} + C^{rr}_{(R)} + C^{\theta\theta}_{(R)} = 0$. This suggests that no curvature terms occur in the turbulence kinetic energy equation.

For the convenience of the derivation of the EASM sensitive to the curvature effect, the curvature term $C^{ij}_{(R)}$ is better written in the Reynolds stress anisotropic form

$$C^{ij}_{(R)} = -2k\frac{U^k}{\sqrt{g_{kk}}}\left[\frac{\partial\left(\ell_n \sqrt{g_{ii} g_{jj}}\right)}{\partial x^k}b^{ij} - \Gamma^i_{kl}\sqrt{\frac{g_{ii}}{g_{ll}}}b^{lj} - \Gamma^j_{kl}\sqrt{\frac{g_{jj}}{g_{ll}}}b^{li}\right.$$

$$\underbrace{\left. + \frac{1}{3}\left(\frac{\partial\left(\ell_n \sqrt{g_{ii} g_{jj}}\right)}{\partial x^k}\delta^{ij} - \Gamma^i_{kl}\sqrt{\frac{g_{ii}}{g_{ll}}}\delta^{lj} - \Gamma^j_{kl}\sqrt{\frac{g_{jj}}{g_{ll}}}\delta^{li}\right)\right]}_{M^{ij}} \tag{19}$$

where b^{ij} is a Reynolds stress anisotropy tensor, that is, $b^{ij} = \overline{u^i u^j}/(2k) - \delta^{ij}/3$. Through the definition of the Christoffel symbol of the second kind, Γ^i_{kl} and Γ^j_{kl}, it can be further deduced that the second line in the preceding expression may be rewritten as

$$M^{ij} = \frac{1}{\sqrt{g_{ii} g_{jj}}}\frac{\partial}{\partial x^k}\left(\sqrt{g_{ii} g_{jj}}\delta_{ij} - g_{ij}\right) \tag{20}$$

This expression shows that M^{ij} has zero trace, consistent with the requirement that $C^{ll}_{(R)} = 0$. What is more significant is that the off-diagonal elements in M^{ij}, that is, $i \neq j$, also equal zero when the coordinate system is orthogonal because the orthogonality suggests $g_{ij} = 0$ for $i \neq j$. Thus, it is seen here that in the orthogonal curvilinear coordinate system $M^{ij} = 0$ and that the curvature terms, as well as the later curvature sensitive ASM, can be greatly simplified.

B. Equilibrium Assumption: ASM

The ASM is based on the assumption that the turbulence anisotropy is in an equilibrium state; mathematically this means the Reynolds stress anisotropy is constant in time and space, $b^{ij} = \text{const}$. In this respect, all of the gradients of b^{ij} vanish. However, the existing ASM is derived on a Cartesian tensor basis in which there is no explicit consideration of the curvature effect. The assumption is often spelled out mathematically as

$$C^{ij} - D^{ij} = (\overline{u^i u^j}/k)\left(C^{(k)} - D^{(k)}\right) \tag{21}$$

that is, the transport of the Reynolds stresses is proportional to that of the turbulence kinetic energy. This expression applies not only to the gradient part but also to the algebraic curvature part of the stress convection that is not necessarily consistent with the equilibrium assumption.

To retain the curvature terms in the stress convection process, a modified approach to the conventional ASM assumption would be

$$C^{ij}_{(G)} - D^{ij} = (\overline{u^i u^j}/k)\left(C^{(k)}_{(G)} - D^{(k)}\right) \tag{22}$$

Here, only the gradient part of the convection term is involved, whereas the curvature terms remain in the equation because they require no modeling. When the assumption in Eq. (22) is adopted rather than the one in Eq. (21), a new ASM retaining the curvature effect in convection can be derived, which reads

$$2Gb^{ij} = \left(P^{ij} - \tfrac{1}{3}\delta^{ij}P^{ll}\right) + \Phi^{ij} + \left(C^{ij}_{(R)} - \tfrac{1}{3}\delta^{ij}C^{ll}_{(R)}\right) \tag{23}$$

where $G = P - \epsilon + C^{ll}_{(R)}/2$. The pressure–strain correlations Φ^{ij} can take any of the model forms available, for example, the Gibson and Launder (GL)[17] model, Launder et al.[18] model, Speziale et al.[19] model, or Fu et al.[20] model. Note that, in the Cartesian coordinate system, the preceding expression is identical to the existing ASM because no curvature terms occur.

C. Explicit Curvature-Sensitive ASM

As discussed before, the orthogonality condition leads to significant simplification in the representation of the curvature terms. The following derivation, thus, takes advantage of the orthogonality condition. To obtain the explicit curvature sensitive ASM in orthogonal form, Eq. (19) is rewritten as

$$C^{ij}_{(R)} = 2[\chi^{ij} b^{ij} + k(b^{il}\Omega^{jl} + b^{jl}\Omega^{il})] \tag{24}$$

where

$$\chi^{ij} = -k\frac{U^k}{\sqrt{g_{kk}}}\frac{\partial \ln\sqrt{g_{ii}g_{jj}}}{\partial x^k}, \qquad \Omega^{ij} = \Gamma^i_{kj}\frac{U^k}{\sqrt{g_{kk}}}\sqrt{\frac{g_{ii}}{g_{jj}}} \tag{25}$$

because $M^{ij} = 0$ in the orthogonal condition. The term Ω^{ij} can be decomposed into two parts, one antisymmetric part, ω^{ij}, and the other a symmetric part, ζ^{ij}, that is,

$$\Omega^{ij} = \omega^{ij} + \zeta^{ij} \tag{26}$$

with

$$\omega^{ij} = \frac{U^k}{2\sqrt{g_{kk}}}\left(\Gamma^i_{kj}\sqrt{\frac{g_{ii}}{g_{jj}}} - \Gamma^j_{ki}\sqrt{\frac{g_{jj}}{g_{ii}}}\right)$$

$$\zeta^{ij} = \frac{U^k}{2\sqrt{g_{kk}}}\left(\Gamma^i_{kj}\sqrt{\frac{g_{ii}}{g_{jj}}} + \Gamma^j_{ki}\sqrt{\frac{g_{jj}}{g_{ii}}}\right) \tag{27}$$

Further derivation shows that the term ζ^{ij} is in fact diagonal, and the following expression can be obtained in the orthogonal coordinate system (Appendix B):

$$\chi^{ij} b^{ij} + k(b^{il}\zeta^{jl} + b^{jl}\zeta^{il}) = 0 \tag{28}$$

Hence, the complexity related to the preceding expression vanishes, leading to a significant simplification in $C^{ij}_{(R)}$ in the curvature-sensitive ASM, that is, Eq. (24) can be reduced to

$$C^{ij}_{(R)} = 2k(b^{il}\omega^{jl} + b^{jl}\omega^{il}) \tag{29}$$

When this expression is substituted and GL or any linear model is adopted for the pressure–strain correlations Φ^{ij} in Eq. (23), the following algebraic equation for b^{ij} can be obtained:

$$2Gb^{ij} = \left[C_2 - \tfrac{4}{3}\right]kS^{ij} + (C_3 - 2)k\left(b^{il}S^{jl} + b^{jl}S^{il} - \tfrac{2}{3}b^{mn}S^{mn}\delta^{ij}\right)$$
$$+ (C_4 - 2)k(b^{il}W^{jl} + b^{jl}W^{il}) - 2k(b^{il}\omega^{jl} + b^{jl}\omega^{il}) \tag{30}$$

where C_1, C_2, C_3, and C_4 are model parameters, whose values are consistent with the model expression for the pressure–strain correlations Φ^{ij}.

Note that S^{ij} is symmetric in i and j and that W^{ij} and ω^{ij} are antisymmetric terms. Following the practice of Gatski and Speziale,[7] Fu et al.,[21] and Rung et al.,[22] the curvature sensitive ASM in the orthogonal form can be expressed explicitly as

$$\overline{u^i u^j} = \tfrac{2}{3}\delta^{ij}k - 2\nu_t\left[S^{ij} + \beta_2(k/\epsilon)(S^{il}W'^{jl} + S^{jl}W'^{il})\right.$$
$$\left. - \beta_3(k/\epsilon)\left(S^{il}S^{lj} - \tfrac{1}{3}\delta^{ij}S^{kl}S^{lk}\right)\right] \tag{31}$$

Here

$$W'^{ij} = W^{ij} - 2\omega^{ij}/(C_4 - 2) \tag{32}$$

$$\nu_t = C^*_\mu k^2/\epsilon, \qquad C^*_\mu = 3\beta_1(1+\eta^2)/[3 + \eta^2 + 6\xi^2(1+\eta^2)]$$

$$\eta^2 = (\beta_3 S)^2/8, \qquad \xi^2 = (\beta_2\Omega)^2/2$$

$$S = (k/\epsilon)\sqrt{2S^{ij}S^{ij}}, \qquad \Omega = (k/\epsilon)\sqrt{2W'^{ij}W'^{ij}}$$

The model coefficients β_1, β_2, β_3, and C_4 take the values 0.095, 0.14, 0.28, and 1.2, respectively, consistent with the GL pressure–strain model. As it appears in expression (31), this is a new nonlinear eddy-viscosity model EASM-C.

Note that, although the orthogonality assumption is adapted in the present derivation to achieve the explicit form of curvature sensitive ASM, extension of this idea to the nonorthogonal formulation, however, is straightforward but much more elaborate.

IV. Model Validation

A. Case Study

In this section, a typical two-dimensional U-type turnaround duct flow,[1] shown in Fig. 1, is chosen as the numerical example to validate the EASM-C. The Reynolds number of the flow is $Re = 10^6$, based on the average inlet flow velocity U_0 and the width of the duct H. In the bend section, the ratio of the outer wall radius to the inner wall radius is 3.

When the EASM-C is applied to the numerical simulation of this flow, the streamwise and normal directions of the flow are chosen as the two computational coordinates, and the whole flowfield is divided into three parts, two planar duct sections and one circular between them. In the planar duct part, the flow governing equation is the Reynolds averaged Navier–Stokes (RANS) equation in the Cartesian (x, y) coordinate system, whereas in the bend the governing equation is written in the polar (θ, r) coordinate system. Because no curvature terms occur explicitly in the Cartesian coordinate system, only the flow transport equations in the polar coordinate system are discussed, that is,

$$\frac{\partial(U^\theta\phi)}{r\partial\theta} + \frac{\partial(rU^r\phi)}{r\partial r} = \frac{\partial}{r\partial\theta}\left(\Gamma_\phi\frac{\partial\phi}{r\partial\theta}\right) + \frac{\partial}{r\partial r}\left(r\Gamma_\phi\frac{\partial\phi}{r\partial r}\right) + S_\phi \tag{33}$$

This equation stands for the continuity, θ-direction momentum, r-direction momentum, turbulent kinetic energy (TKE), and TKE dissipation rate equation, when ϕ is taken as 1, U^θ, U^r, k, and ϵ, respectively. Γ_ϕ is the diffusion coefficient of the transport variable ϕ, and S_ϕ is the source term. In particular, for EASM-C, the curvature effect term ω^{12} (or $\omega^{\theta r}$) defined in Eq. (27) takes the form

$$\omega^{12} = -\omega^{21} = U^\theta/r \tag{34}$$

and this effect is included in the source term of S_ϕ ($\phi = U^\theta, U^r, k, \epsilon$).

In the numerical solution process, the RANS is solved on a nonstaggered H-type grid system. The convection and diffusion terms in RANS are discretized with a second-order accurate Zhu's[23] and a central difference scheme, respectively. To obtain the pressure field, the SIMPLE algorithm, in conjunction with the momentum-interpolation technique, has been adopted to treat the pressure–velocity coupling on the nonstaggered grid system. To ensure numerical accuracy, a grid-independence study was performed. Two sets of grid systems, that is, a 270×100 grid and a 350×200 grid, have been used for computation, and negligible difference was detected in their final results. Then, the fine grid was used to minimize the truncation errors in the separated flow region. In terms of the computational boundary conditions, the inlet conditions are specified with the experimental data of Monson et al.[1] The wall function is applied to both the inner and the outer wall of this turnaround duct to bridge the gap between the logarithmic layer and the wall. At the exit boundary, the partial difference of all of the flow variables along

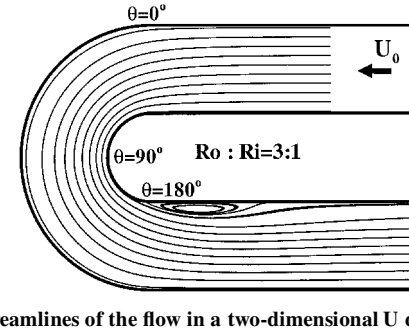

Fig. 1 Streamlines of the flow in a two-dimensional U duct (obtained with EASM-C).

the streamwise direction is set to zero. The convergence criterion of computation is taken as a four-decade drop of rms residual of the continuity and momentum equations and 2.5-decade drop of rms residual of the ϵ equation.

B. Numerical Results and Discussion

With the aforementioned numerical method, the numerical results of two turbulence models, the EASM proposed by Gatski and Speziale,[7] and the EASM-C developed in this work, are presented here. These results are also compared with the experimental (Exp) results of Monson et al.[1] and the numerical results of the Reynolds stress model (RSM) obtained from Luo and Lakshminarayana.[9]

The flow around the two-dimensional U duct is generally featured in Fig. 1 and shows the computed streamlines with the EASM-C. The predicted and experimental profiles of the streamwise velocity U, the turbulence kinetic energy k, and the Reynolds shear stress τ^{12} at three stations, that is, $\theta = 0$, $\theta = 30$, and $\theta = 90$ deg are shown in Figs. 2a–2c, where the results of EASM, EASM-C, RSM, and Exp. are drawn with solid lines, dotted lines, dashed lines, and circles, respectively. At station $\theta = 0$ deg, where the bend begins, the mean velocity profiles predicted by all of the models are in agreement with the experimental data. For the k profiles, EASM and EASM-C yield similar results in that they agree with the experimental data at the concave wall but overpredict the magnitude of k near the convex wall to a large extent. For the shear stress profile, the EASM and EASM-C exhibit a big difference in that the EASM even predicts a wrong sign for τ^{12} near the convex wall.

As the flow reaches position $\theta = 30$ deg into the bend, the curvature of the bend exerts significant influence on the turbulence level of the flow. The flow turbulence is strongly suppressed near the convex wall, whereas turbulence enhancement occurs near the concave wall. The EASM fails to reflect the curvature effect, greatly overpredicting the turbulence energy and shear stress level at the convex wall, whereas the results of EASM-C seem better. The EASM-C captures a significant suppression of k and τ^{12} profiles near the convex wall and is in good agreement with the experimental data. The superiority of the EASM-C to the EASM should be purely attributed to the curvature modification in the EASM-C. For the outer wall, the results of EASM, EASM-C, and RSM all fall within the the error band of the experiment, and it is difficult to decide whether the EASM-C is more capable of treating the curvature effect near the concave wall.

At position $\theta = 90$ deg, the major features of the flow are similar to those observed at $\theta = 30$ deg. The EASM-C results follow the curvature effects quite well as the flow turns around, although the turbulence enhancement at the concave surface is underpredicted, in a manner similar to the RSM results. Again, the EASM results show less sensitivity to the bend than EASM-C and RSM results, significantly overpredicting k and τ^{12} levels at the convex surface. The underprediction of the maximum level of turbulence for all three models is likely caused by the inadequacy of the pressure–strain model and the ϵ equation to account for the large-scale vortex structures in concave curved flow.[9] The benefit of the EASM-C to treat the curvature effect near the concave wall is now hard to determine.

Shown in Figs. 3a–3c are predicted and experimental profiles of the streamwise velocity U, the turbulence kinetic energy k, and the Reynolds shear stress τ^{12} at the other two stations, that is, $\theta = 180$ deg and $x = 2h$ downstream of the bend. In fact, the flow encounters an adverse pressure gradient on the inner convex wall and a favorable pressure gradient on the outer concave wall downstream of $\theta = 90$ deg. Because of the severe adverse pressure gradient, as well as highly diminished turbulent shear stress, the boundary layer separates in the experiment[1] around $\theta = 150$ deg on the convex wall and extends to $x/H = 1.2$–1.5 downstream of the end of bend, with mean maximum height of $0.14H$. Both the EASM-C and EASM predict this flow recirculation accurately. The computed flowfield streamlines with EASM-C (Fig. 1) indicate that the flow separates near $\theta = 172$ deg and reattaches at $x/H = 1.2$ downstream of the end of bend, with maximum bubble height of $0.15H$. However, there is a significant discrepancy between the numerical and the

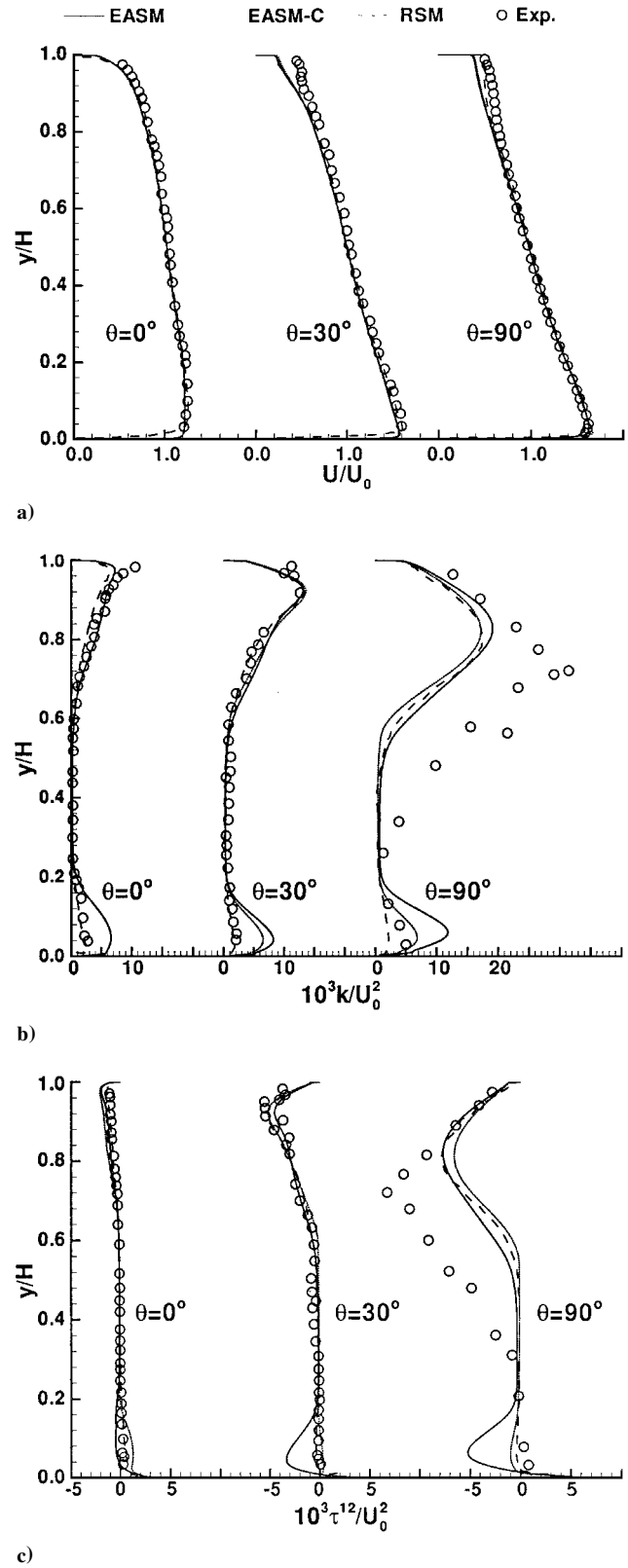

Fig. 2 Profiles at $\theta = 0$, 30, and 90 deg, turnaround duct case, $Re = 10^6$.

experimental results in the turbulence quantities at the end of the bend. The experimental data show a very strong peak in k and τ^{12} profiles in the vicinity of the separating streamline ($\theta = 180$ deg) at the convex surface. This flow behavior is not captured by any of the turbulence models here. These large peak values in k and τ^{12} had been considered to result from the large unsteadiness of the separation bubble, as observed in the experiment of Monson et al.[1] At $x/H = 2$ downstream of the end of the bend, the flow has reattached

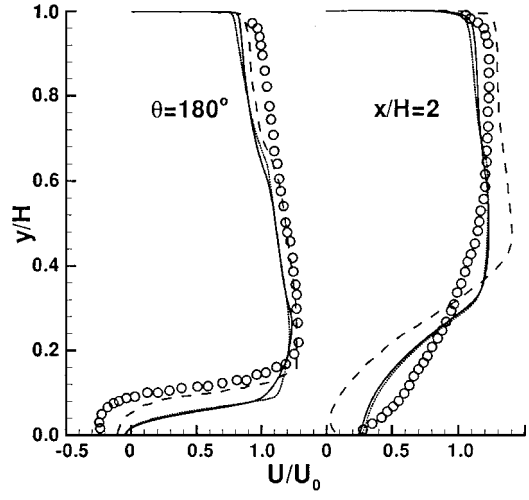

a)

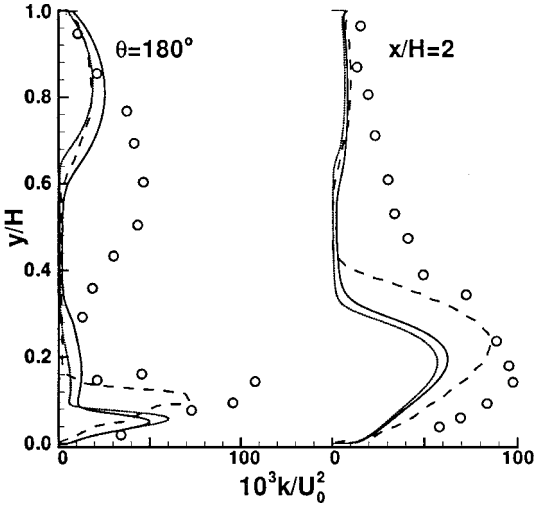

b)

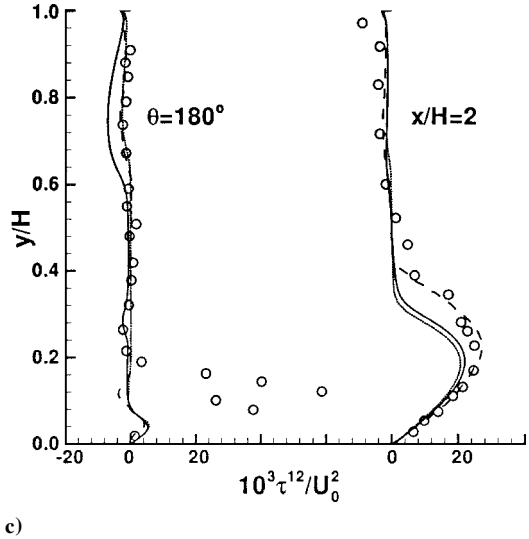

c)

Fig. 3 Profiles at $\theta = 180$ deg and $x/H = 2$, turnaround duct case, $Re = 10^6$.

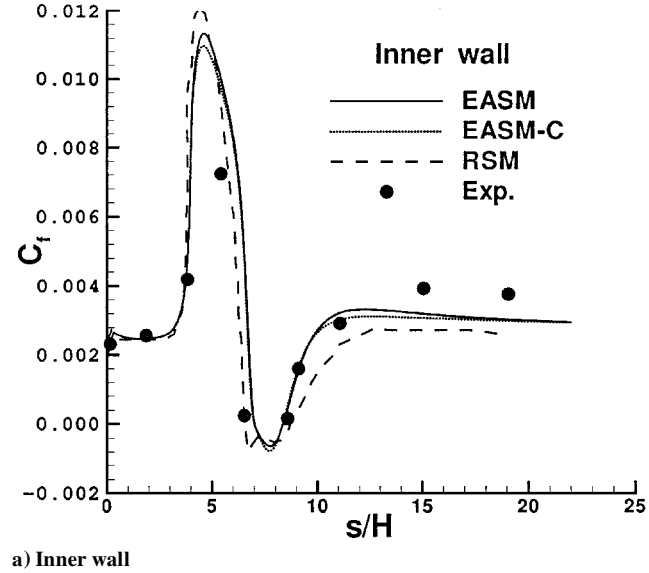

a) Inner wall

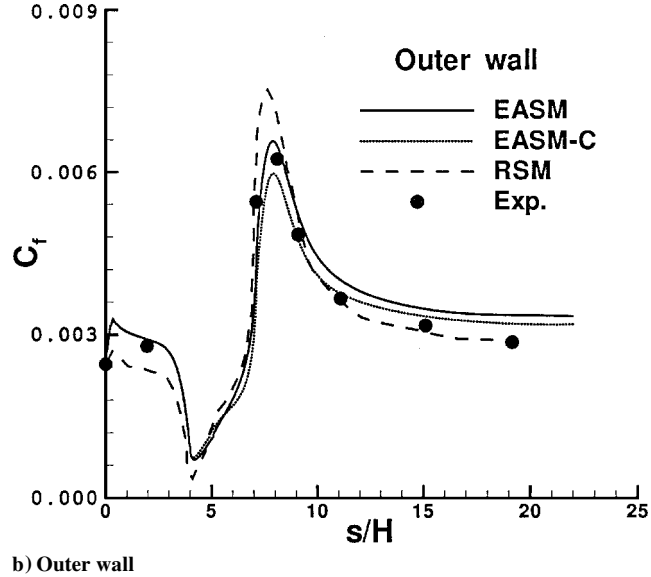

b) Outer wall

Fig. 4 Wall skin-friction coefficients, turnaround duct case, $Re = 10^6$.

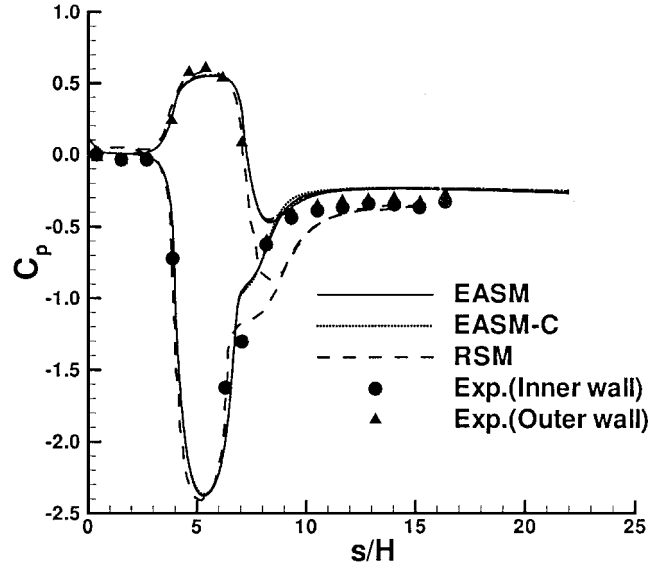

Fig. 5 Wall static pressure coefficients, turnaround duct case, $Re = 10^6$.

and started to recover. All of the computed profiles of k and τ^{12} follow the measurement data, but a significant difference occurs as a result of the unsteadiness of the recirculation bubble.

Shown in Figs. 4 and 5 are the comparisons of the friction and pressure coefficients along the inner and outer walls (where s is the arc length to the inlet). It is seen from Figs. 4 and 5 that the result of EASM-C is close to that of EASM; both results nearly separate and reattach in the same location. However, further referencing the numerical data, a slight improvement can be detected, that is, the flow calculated with EASM-C separates near $\theta = 172$ deg and reattaches at $x/H = 1.2$ downstream of the end of bend as stated before, whereas the flow calculated with EASM separates near $\theta = 174$ deg and reattaches at $x/H = 1.25$ downstream of the end of bend. This improvement of curvature modification is not as significant as that of shear stress profile, and it may be attributed to the wall function approach used in the numerical process.

The preceding numerical comparisons of the models' performance in the two-dimensional U-duct flow clearly validated the argument underlining the EASM-C. To further understand the physical reasoning behind the EASM-C, it is appropriate to highlight the curvature effects on the explicit constitutive relation for the Reynolds shear stress τ^{12}. From Eq. (31),

$$\tau^{12} = -2\nu_t\left\{S^{12} - (k/\epsilon)\left[\beta_2(S^{11} - S^{22})W'^{12} + \beta_3 S^{1l}S^{l1}\right]\right\} \quad (35)$$

Here, the effective vorticity term W' can be written as

$$W'^{12} = W^{12} + \frac{2}{2 - C_4}\omega^{12} = \frac{1}{2}\left(\frac{\partial U^r}{r\partial\theta} - \frac{\partial U^\theta r}{r\partial r}\right) + \frac{2}{2 - C_4}\frac{U^\theta}{r} \quad (36)$$

Thus, the curvature term ω^{12} introduced can be considered as an apparent vorticity in the preceding expression modifying $\partial U^\theta r/r\partial r$. It is clear that at the convex surface these two terms have the same positive sign, suggesting a diminishing effect on W'^{12}, whereas at the concave wall, $\partial U^\theta r/r\partial r$ turns negative and the net effect on W'^{12} is enhancement that leads to increased level in τ^{12}. This behavior is the underlining mechanism that improves the performance of the EASM-C.

C. Two Other Cases

Two additional cases are tested. First, the flow with a configuration similar to that discussed in last section is reconsidered. However, now the Reynolds number of the flow is $Re = 2.1 \times 10^5$. EASM and EASM-C models are used to simulate this flow, and the computations are performed on the 270×100 coarse grid for simplicity. The predicted profiles of the turbulence kinetic energy k and the

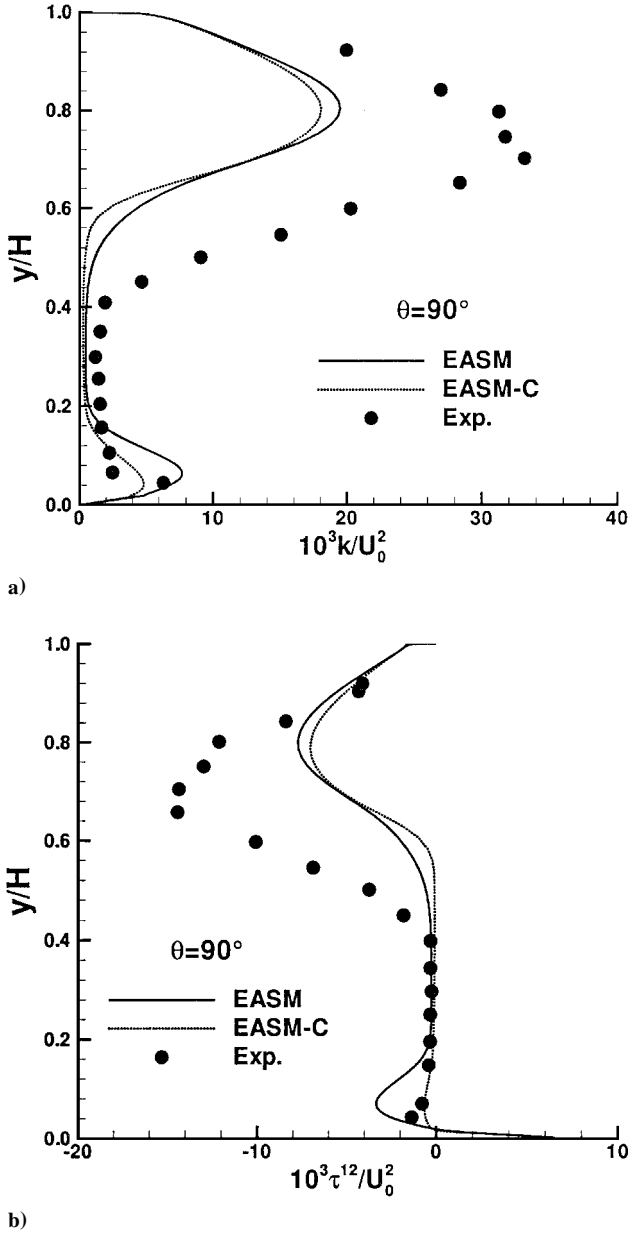

Fig. 6 Profiles of shear stress and TKE at $\theta = 90$ deg, turnaround duct case, $Re = 2.1 \times 10^5$.

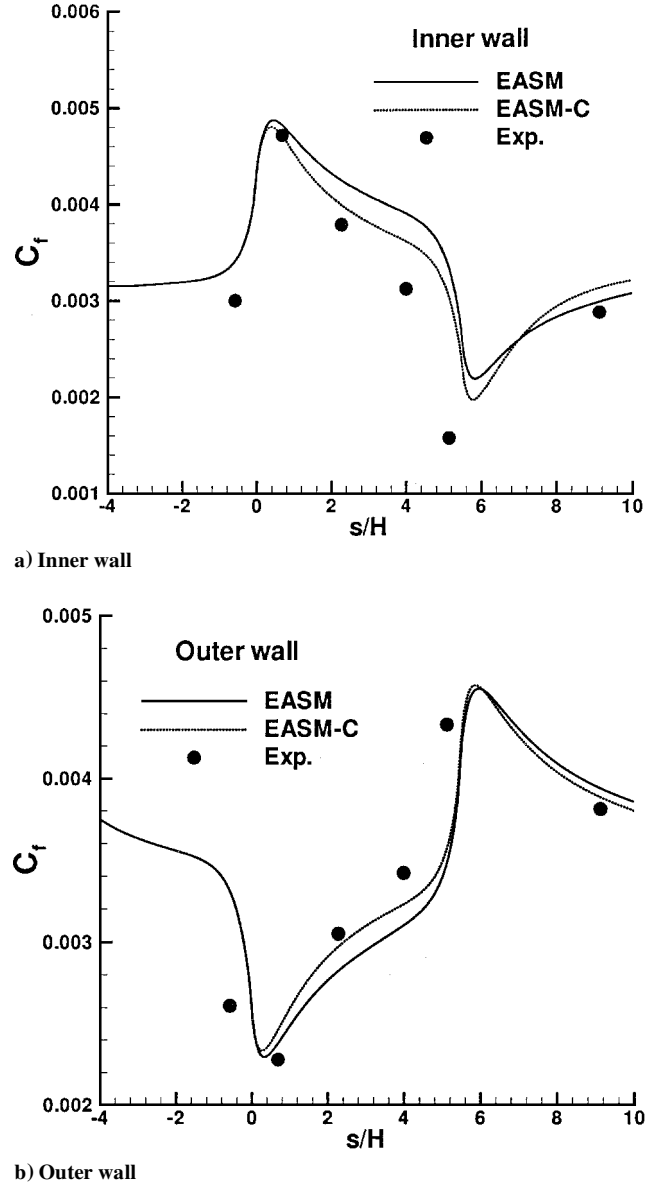

Fig. 7 Wall skin-friction coefficients, 90-deg bend case, $Re = 2.2 \times 10^5$.

Reynolds shear stress τ^{12} at the $\theta = 90$ deg station are compared to experimental results[2] in Figs. 6a and 6b. It is shown that the result is close to that presented in Figs. 2b and 2c. Under this circumstance, the EASM-C also captures the damping effect of curvature at the concave wall well, but underpredicts the turbulence enhancement at the concave surface.

Second, a 90-deg bend is investigated. In the circular section, the ratio of the outer wall radius to the inner wall radius is 4:3. The Reynolds number of the flow is $Re = 2.2 \times 10^5$. The EASM and EASM-C are used to solve this flow, and the computations are also performed on the 270×100 coarse grid. The calculated friction coefficients along the inner and outer wall of the bend are compared to experimental values[24] in Figs. 7a and 7b. It can be seen that the result of EASM-C is somewhat closer to the experimental result than EASM, and this improvement is surely attributed to the curvature modification in the EASM-C.

V. Conclusions

Through the analysis of the Reynolds stress transport equations written in a curvilinear coordinate system and the identification of the curvature terms in the stress convection, the present work formulated a curvature sensitive algebraic stress model. This model is rigorously transformed into an explicit Reynolds stress constitutive relation, EASM-C, which is, effectively, a nonlinear eddy-viscosity model. The curvature sensitivity in the EASM-C is introduced in the form of effective vorticity, which is modified with the curvature-related terms. It is observed in the numerical validation of the model, calculations of the two-dimensional U duct and 90-deg bend flow, that the EASM-C is indeed able to capture the turbulence suppression at the convex surface, which had only been resolved, previously, with the RSM, the full second-moment closure. The present EASM-C, thus, provides a simple but effective alternative approach to the traditional RSM to capture the flow curvature effects. However, for the concave surface, the ability of EASM-C to capture the turbulence enhancement effect is hard to determine from the available data. Because the turbulence enhancement effect is been believed to be driven by a three-dimensional effect, three-dimensional computation is needed to check the rationale of the EASM-C further.

Appendix A: Derivation of Equation (17)

In orthogonal curvilinear coordinate system, $g^{ij} = g_{ij} = 0$ if $i \neq j$, and $\Gamma^i_{jk} = g^{ir}\Gamma_{jkr} = g^{ii}\Gamma_{jki}$. Thus,

$$C^{ll}_{(R)} = -\frac{U^k}{\sqrt{g_{kk}}}\left(\overline{u^l u^l}\frac{\partial(\ell_n g_{ll})}{\partial x^k} - \frac{2\Gamma_{ksl}\overline{u^s u^l}}{\sqrt{g_{ll}g_{ss}}}\right)$$

$$= -\frac{U^k}{\sqrt{g_{kk}}}\left[\overline{u^l u^l}\frac{\partial(\ell_n g_{ll})}{\partial x^k} - \frac{2\Gamma_{kll}\overline{u^l u^l}}{\sqrt{g_{ll}g_{ll}}}\right.$$

$$\left. - \left(\frac{\Gamma_{kls}\overline{u^l u^s}}{\sqrt{g_{ss}g_{ll}}} + \frac{\Gamma_{ksl}\overline{u^s u^l}}{\sqrt{g_{ll}g_{ss}}}\right)_{s\neq l}\right]$$

When the identities $\partial g_{ij}/\partial x^k = \Gamma_{jki} + \Gamma_{ikj}$ and $\partial g_{ll}/\partial x^k = 2\Gamma_{kll}$ are substituted into the preceding equation and the sum index s, l is rewritten to be i, j, the preceding equation is simplified as

$$C^{ll}_{(R)} = -\frac{U^k}{\sqrt{g_{kk}}}\left[\overline{u^l u^l}\frac{\partial(\ell_n g_{ll})}{\partial x^k} - \frac{2\Gamma_{kll}\overline{u^l u^l}}{g_{ll}} - \left(\frac{\Gamma_{kji}\overline{u^i u^j}}{\sqrt{g_{ii}g_{jj}}}\right.\right.$$

$$\left.\left. + \frac{\Gamma_{kij}\overline{u^j u^i}}{\sqrt{g_{jj}g_{ii}}}\right)_{i\neq j}\right] = \frac{U^k}{\sqrt{g_{kk}}}\left[2\frac{\overline{u^i u^j}}{\sqrt{g_{ii}g_{jj}}}\frac{\partial g_{ij}}{\partial x^k}\right]_{i\neq j} = 0$$

Appendix B: Derivation of Equation (28)

First, with the expression $\Gamma^i_{jk} = g^{ir}\Gamma_{jkr} = g^{ii}\Gamma_{jki}$ in the orthogonal coordinate system, ζ^{ij} can be rewritten as

$$\zeta^{ij} = \frac{U^k}{2\sqrt{g_{kk}}}\left(\sqrt{\frac{g_{ii}}{g_{jj}}}\Gamma^i_{kj} + \sqrt{\frac{g_{jj}}{g_{ii}}}\Gamma^j_{ki}\right)$$

$$= \frac{U^k}{2\sqrt{g_{kk}}}\frac{1}{\sqrt{g_{ii}g_{jj}}}(\Gamma_{kji} + \Gamma_{kij}) = \frac{U^k}{2\sqrt{g_{kk}}}\frac{1}{\sqrt{g_{ii}g_{jj}}}\frac{\partial g_{ij}}{\partial x^k}$$

$$= \begin{cases} \dfrac{U^k}{2\sqrt{g_{kk}}}\dfrac{1}{g_{ii}}\dfrac{\partial g_{ii}}{\partial x^k} & (\text{if} \quad i = j) \\ 0 & (\text{if} \quad i \neq j) \end{cases}$$

Thus, ζ^{ij} has diagonal elements only.

Second, when ζ^{ij} is considered diagonal, the expression for $\chi^{ij}b^{ij} + k(b^{il}\zeta^{jl} + b^{jl}\zeta^{il})$ can be simplified as

$$\chi^{ij}b^{ij} + k(b^{il}\zeta^{jl} + b^{jl}\zeta^{il})$$

$$= b^{ij}\chi^{ij} + kb^{ij}\zeta^{jj} + b^{ji}\zeta^{ii}$$

(when $i \neq j$, $\zeta^{ij} = 0$, and no summation on i and j)

$$= b^{ij}(\chi^{ij} + k\zeta^{jj} + k\zeta^{ii})$$

$$= kb^{ij}\frac{U^k}{\sqrt{g_{kk}}}\left(-\frac{1}{\sqrt{g_{ii}g_{jj}}}\frac{\partial\sqrt{g_{ii}g_{jj}}}{\partial x^k} + \frac{1}{2g_{ii}}\frac{\partial g_{ii}}{\partial x^k} + \frac{1}{2g_{jj}}\frac{\partial g_{jj}}{\partial x^k}\right)$$

$$= kb^{ij}\frac{U^k}{\sqrt{g_{kk}}}\left[-\frac{1}{2g_{ii}g_{jj}}\frac{\partial(g_{ii}g_{jj})}{\partial x^k} + \frac{1}{2g_{ii}g_{jj}}\frac{\partial(g_{ii}g_{jj})}{\partial x^k}\right]$$

$$= 0$$

Therefore, the term relating to χ^{ij} and ζ^{ij} in Eq. (24) vanishes.

Acknowledgment

This work is supported by the NSF of China through Grant 1972508.

References

[1]Monson, D. J., Seegmiller, H. L., McConnaughey, P. K., and Chen, Y. S., "Comparison of Experiment with Calculations Using Curvature-Corrected Zero and Two-Equation Turbulence Models for a Two-Dimensional U Duct," AIAA Paper 90-1484, 1990.

[2]Sandborn, V. A., and Shin, J. C., "Water Flow Measurements in a 180 Degree Turn-Around Duct," NASA CR NAS8-36354, 1989.

[3]So, R. M. C., and Mellor, G. L., "Experiment on Convex Curvature Effects in Turbulent Boundary Layers," *Journal of Fluid Mechanics*, Vol. 60, 1973, pp. 43–62.

[4]Launder, B. E., and Loizou, P. A., "Laminarization of Three Dimensional Accelerating Boundary Layers in a Curved Rectangular-Sectioned Duct," *International Journal of Heat and Fluid Flow*, Vol. 13, No. 2, 1992, pp. 124–131.

[5]Craft, T. J., Launder, B. E., and Suga, K., "Development and Application of a Cubic Eddy-Viscosity Model of Turbulence," *International Journal of Heat and Fluid Flow*, Vol. 17, No. 2, 1996, pp. 108–115.

[6]Pope, S. B., "A More General Effective Viscosity Hypothesis," *Journal of Fluid Mechanics*, Vol. 72, 1975, pp. 331–340.

[7]Gatski, T. B., and Speziale, C. G., "On Explicit Algebraic Stress Models for Complex Turbulent Flows," *Journal of Fluid Mechanics*, Vol. 254, 1993, pp. 59–78.

[8]Rumsey, C. L., Gatski, T. B., and Morrison, J. H., "Turbulence Model Predictions of Strongly Curved Flow in a U Duct," *AIAA Journal*, Vol. 38, No. 8, 2000, pp. 1394–1402.

[9]Luo, J., and Lakshminarayana, B., "Prediction of Strongly Curved Turbulent Duct Flows with Reynolds Stress Model," *AIAA Journal*, Vol. 35, No. 1, 1997, pp. 91–98.

[10]Rumsey, C. L., Gatski, T. B., Anderson, W. K., and Nielsen, E. J., "Isolating Curvature Effects in Computing Wall-Bounded Turbulent Flows," *International Journal of Heat and Fluid Flow*, Vol. 22, No. 6, 2001, pp. 573–582.

[11]Rodi, W., and Scheurer, G., "Calculation of Curved Shear Layers with Two Equation Turbulence Models," *Physics of Fluids*, Vol. 26, No. 6, 1983, pp. 1422–1436.

[12]Girimaji, S. S., "A Galilean Invariant Explicit Algebraic Reynolds Stress Model for Curved Flows," ICASE, Rept. 96-38, Hampton, VA, 1996.

[13]Wallin, S., and Johansson, A. V., "Modelling of Streamline Curvature Effects on Turbulence in Explicit Algebraic Reynolds Stress Turbulence Models," *Turbulence and Shear Flow Phenomena, Second International Symposium*, Vol. 1, KTH, Stockholm, 2001, pp. 223–228.

[14]Fu, S., Huang, P. G., Launder, B. E., and Leschziner, M. A., "A Comparison of Algebraic and Differential Second-Moment Closure for Axisymmetric Turbulent Shear Flows With and Without Swirls," *Journal of Fluids Engineering*, Vol. 110, No. 2, 1988, pp. 216–221.

[15]Gibson, M. M., and Younis, B. A., "Calculation of Swirling Jets with a Reynolds Stress Closure," *Physics of Fluids*, Vol. 29, No. 1, 1986, pp. 38–48.

[16]Sokolnikoff, I. S., *Tensor Analysis*, Wiley, New York, 1964, pp. 146–173.

[17]Gibson, M. M., and Launder, B. E., "Ground Effect on Pressure Fluctuation in the Atmospheric Boundary Layer," *Journal of Fluid Mechanics*, Vol. 86, 1978, pp. 491–511.

[18]Launder, B. E., Reece, G. J., and Rodi, W., "Progress in the Development of a Reynolds-Stress Turbulence Closure," *Journal of Fluid Mechanics*, Vol. 68, 1975, pp. 537–566.

[19]Speziale, C. G., Sarkar, S., and Gatski, T. B., "Modelling the Pressure Strain Correlation of Turbulence: an Invariant Dynamical System Approach," *Journal of Fluid Mechanics*, Vol. 227, 1991, pp. 245–272.

[20]Fu, S., Launder, B. E., and Tselepidakis, D. P., "Accommodating the Effects of High Strain Rates in Modelling the Pressure-Strain Correlation," Dept. of Mechanical Engineering, Rept. TFD/87/5, Univ. of Manchester Inst. of Science and Technology, Manchester, England, U.K., 1987.

[21]Fu, S., Rung, T., and Thiele, F., "Realizability of the Nonlinear Stress–Strain Relationships for Reynolds-Stress Closures," *Turbulent Shear Flows 11*, INPG, Grenoble, France, 1997, pp. 13.1–13.6.

[22]Rung, T., Thiele, F., and Fu, S., "On the Realizability of Nonlinear Stress–Strain Relationships for Reynolds-Stress Closures," *Flow, Turbulence and Combustion*, Vol. 60, No. 4, 1999, pp. 333–359.

[23]Zhu, J., "A Low-Diffusive and Oscillation-Free Convection Scheme," *Communications in Applied Numerical Methods*, Vol. 7, No. 3, 1991, pp. 225–232.

[24]Luo, J., and Lakshminarayana, B., "Analysis of Streamline Curvature Effects on Wall-Bounded Turbulent Flows," *AIAA Journal*, Vol. 35, No. 8, 1997, pp. 1273–1279.

R. M. C. So
Associate Editor